Heliyon 10 (2024) e29331

Contents lists available at ScienceDirect

Heliyon

journal homepage: www.cell.com/heliyon

Research article

Improving radiomic modeling for the identification of symptomatic carotid atherosclerotic plaques using deep learning-based 3D super-resolution CT angiography

Lingjie Wang [a], Tiedan Guo [a], Li Wang [a], Wentao Yang [b], Jingying Wang [c], Jianlong Nie [d], Jingjing Cui [d], Pengbo Jiang [d], Junlin Li [e], Hua Zhang [a,*]

[a] Department of Medical Imaging, First Hospital of Shanxi Medical University, Taiyuan, Shanxi Province, 030001, China
[b] Basic Medical College, Shanxi Medical University, Taiyuan, Shanxi Province, 030001, China
[c] Department of Endemic Disease Prevention and Control, Shanxi Province Disease Prevention and Control Center, Shanxi Province, 030001, China
[d] Shanghai United Imaging Intelligence, Co., Ltd., Shanghai City, 200030, China
[e] Department of Imaging Medicine, Inner Mongolia Autonomous Region People's Hospital, Hohhot, 010017, China

ARTICLE INFO

Keywords:
Deep learning
Super-resolution
Radiomics
Computed tomography angiography
Carotid plaques

ABSTRACT

Rationale and objectives: Radiomic models based on normal-resolution (NR) computed tomography angiography (CTA) images can fail to distinguish between symptomatic and asymptomatic carotid atherosclerotic plaques. This study aimed to explore the effectiveness of a deep learning-based three-dimensional super-resolution (SR) CTA radiomic model for improved identification of symptomatic carotid atherosclerotic plaques.

Materials and methods: A total of 193 patients with carotid atherosclerotic plaques were retrospectively enrolled and allocated into either a symptomatic (n = 123) or an asymptomatic (n = 70) groups. SR CTA images were derived from NR CTA images using deep learning-based three-dimensional SR technology. Handcrafted radiomic features were extracted from both the SR and NR CTA images and three risk models were developed based on manually measured quantitative CTA characteristics and NR and SR radiomic features. Model performances were assessed via receiver operating characteristic, calibration, and decision curve analyses.

Results: The SR model exhibited the optimal performance (area under the curve [AUC] 0.820, accuracy 0.802, sensitivity 0.854, F1 score 0.847) in the testing cohort, outperforming the other two models. The calibration curve analyses and Hosmer–Lemeshow test demonstrated that the SR model exhibited the best goodness of fit, and decision curve analysis revealed that SR model had the highest clinical value and potential patient benefits.

Conclusions: Deep learning-based three-dimensional SR technology could improve the CTA-based radiomic models in identifying symptomatic carotid plaques, potentially providing more accurate and valuable information to guide clinical decision-making to reduce the risk of ischemic stroke.

Abbreviations: AUC, area under the curve; CTA, computed tomography angiography; NR, normal-resolution; SR, super-resolution; 3D, three-dimensional.

* Corresponding author. First Hospital of Shanxi Medical University, No. 85, Jiefang South Road, Taiyuan, Shanxi, 03001, China.
E-mail address: 13623665879@163.com (H. Zhang).

https://doi.org/10.1016/j.heliyon.2024.e29331
Received 6 January 2024; Received in revised form 4 April 2024; Accepted 5 April 2024
Available online 9 April 2024

1. Introduction

Carotid atherosclerosis-associated ischemic stroke accounts for 10–15% of all ischemic stroke cases worldwide [1]. Ischemic stroke caused by carotid atherosclerotic plaques results from insufficient perfusion due to luminal stenosis, as well as acute vascular occlusion caused by embolism or plaque rupture [2,3]. Although current guidelines still predominantly use the degree of stenosis as a clinical decision-making criterion for ischemic stroke prevention strategies in patients with carotid plaque [4–7], certain characteristics of the carotid plaque itself, including those related to its morphology and composition, are also associated with stroke risk, independent of the degree of luminal stenosis [8–10].

Symptomatic patients with carotid atherosclerotic plaques are more likely than asymptomatic patients to experience ischemic stroke [4,11]. Symptomatic carotid plaques appear to play a significant role in atherosclerotic stroke risk, and early diagnosis based on accurate plaque information is crucial for early intervention, treatment, and prevention of ischemic stroke and related deaths [2,12].

Computed tomography angiography (CTA) is often used in the rapid evaluation of the degree of carotid luminal stenosis and detection of carotid plaques [10]. However, the spatial resolution of CTA images is often negatively impacted by hardware limitations, acquisition time, and radiation exposure, impairing physicians' ability to provide a precise diagnosis and treatment. Furthermore, low image resolution can lead to inaccurate plaque border delineation and make fine spatial details of intraplaque components difficult to distinguish, especially for smaller plaques, significantly affecting the accuracy of plaque risk assessments.

Therefore, the spatial resolution in medical imaging must be improved to facilitate accurate assessments and disease prediction. Conventional interpolation methods for enhancing image resolution inevitably lead to blurred edges and blocking artifacts [13]. In recent years, deep learning-based super-resolution (SR) reconstruction techniques have provided an end-to-end training approach for improving image resolution, and promising results have been observed in enhancing the spatial resolution of medical images in many modalities [13,14], including neuroimaging, chest and abdominal imaging, and fluorescence microscopy [13,15–17].

Radiomics is an image analysis technique for extracting and statistically analyzing highly quantitative mineable data that would otherwise be invisible to the naked eye on digital medical images, facilitating accurate disease diagnoses, guiding clinical decision-making, and improving prognostic evaluations and clinical outcome predictions [18–20]. Radiomics have been utilized to

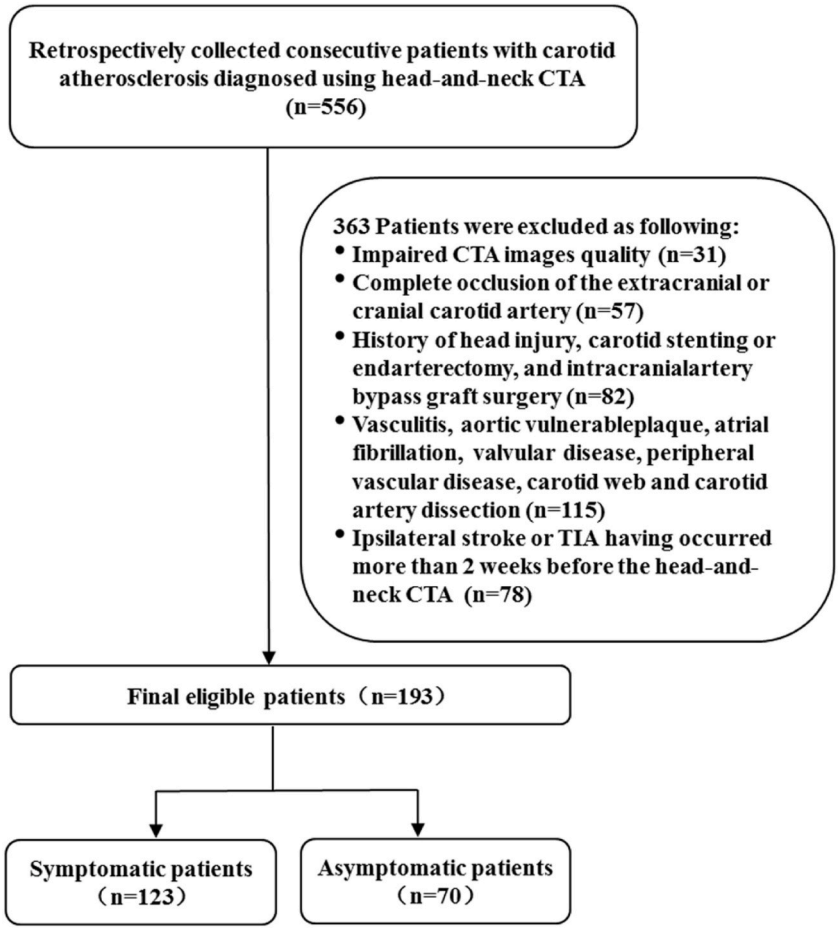

Fig. 1. Flowchart of patient recruitment.

effectively predictive the risk of ischemic stroke based on quantitative analyses of intraplaque compositions [21–23]. Although radiomic features can still be affected by low pixel density in a region of interest, deep learning-based image reconstruction can significantly improve the robustness of important radiomic features [24,25].

The aim of this study was to generate and evaluate a model based on a three-dimensional (3D) SR reconstruction technique for improving medical image quality, utilizing a generative adversarial network as the basic architecture. More specifically, we aimed to analyze differences in radiomic characteristics between symptomatic and asymptomatic carotid plaques using deep learning-based SR reconstructed carotid CTA images and to evaluate whether this technique can improve the diagnostic performance of methods for predicting symptomatic plaques in carotid CTA.

2. Materials and methods

2.1. Patient population, ethics approval, and definitions

This study retrospectively analyzed data from consecutive patients diagnosed with carotid atherosclerosis via head-and-neck CTA in our hospital from January 1, 2018, to December 31, 2021. Institutional review board approval (no. 2018K008) was obtained, and the requirement for informed consent was waived because of the retrospective design. The detailed inclusion/exclusion criteria are shown in Supplementary E1, and patient selection flowchart is shown in Fig. 1.

Symptomatic carotid plaque was defined as the presence of ipsilateral acute ischemic symptoms in the distribution of the anterior and middle cerebral arteries, including cases of transient ischemic attack and ischemic stroke. Transient ischemic attack was diagnosed as a brief episode of neurologic dysfunction, including monocular amaurosis fugax, dysarthria, and dysphasia, in the absence of evidence of acute cerebral infarction on medical imaging and with resolution of signs and symptoms within 24 h [26].

Stroke was defined as clinical evidence of cerebral or retinal focal ischemic injury based on symptoms persisting for ≥24 h [27]. Diffusion-weighted imaging was used, and only patients with diffusion-weighted imaging-positive embolic infarcts in the ipsilateral carotid territory were included in the symptomatic group.

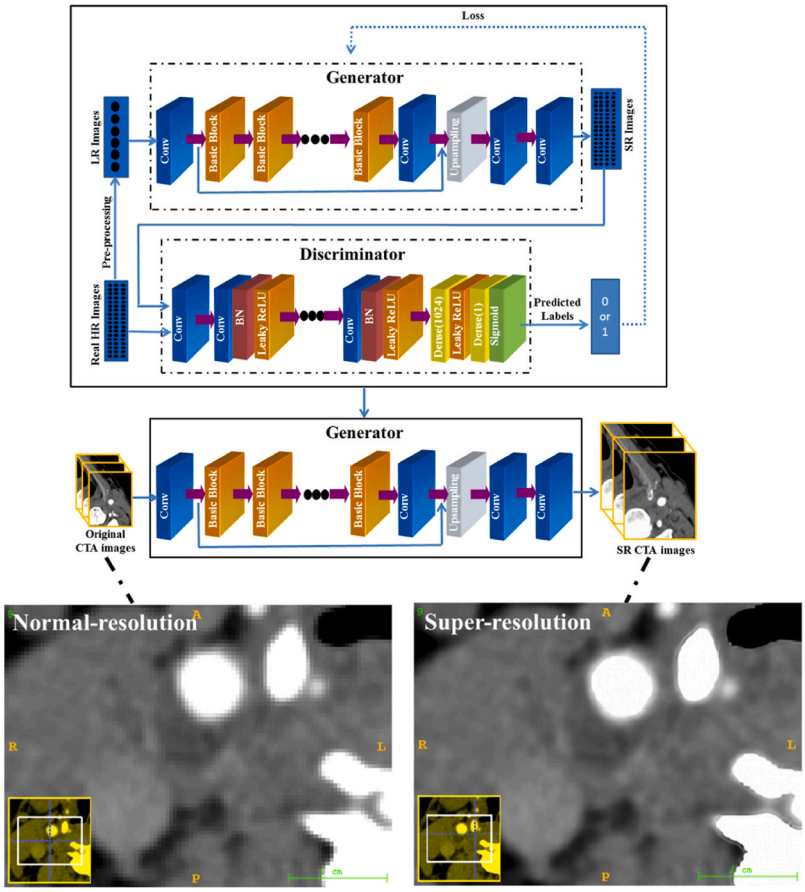

Fig. 2. Diagram of generative adversarial networks used to generate super-resolution CTA images from normal-resolution CTA images. CTA, computed tomography angiography.

2.2. CTA image acquisition

Head-and-neck CTA was performed using a third-generation dual-source scanner (SOMATOM Force; Siemens Healthcare, Erlangen, Germany). The detailed scanning protocol is shown in Supplementary E2. All obtained scan data were transferred to a dedicated post-processing workstation (syngo.via, version VB10B; Siemens Healthcare).

2.3. Conventional CTA-derived carotid plaque analysis

On the post-processing workstation, CTA images were evaluated and measured. The locations of carotid plaques included the common carotid artery, carotid bifurcation (including a range of 2 cm above and below the bifurcation), and extracranial internal carotid artery. Atherosclerotic plaque at the narrowest point in the carotid artery was selected as the object of study, and its thickness, length, area, minimum luminal area, degree of stenosis, and CT attenuation were measured.

The maximum plaque thickness was measured in the axial plane. The measurement method for CT attenuation involved manually drawing a 1–2-mm^2 region of interest in the axial plane and placing it on the thickest section of the plaque, avoiding contact with intraluminal or adventitial calcifications to minimize partial volume effects. Measurements were also performed on the two adjacent sections above and below the chosen section using the same method, with the average of the three measurements used as the final CT attenuation value. The plaque length, minimum luminal area, and degree of stenosis were measured and recorded on the curved planar reconstruction images. The degree of carotid artery stenosis was calculated according to the methods described in the North American Symptomatic Carotid Endarterectomy Trial, using the following formula:

Degree of stenosis (%) = (dilated segment normal arterial diameter – residual lumen diameter at the stenotic segment)/dilated segment normal arterial diameter × 100% [28].

In addition, intra-plaque ulceration was assessed and recorded. Ulceration was defined as contrast enhancement on CTA extending at least 1 mm beyond the blood vessel lumen in at least two planes [29]. Two radiologists with 5 and 12 years of experience in cardiovascular imaging evaluated the qualitative criteria; any disagreements were discussed until a consensus was reached.

2.4. Deep-learning SR networks

As its basic architecture, the 3D SR reconstruction technique employed in this study utilized a generative adversarial network, which is a type of deep learning model comprising a generator network and a discriminator network [30]; the former produces high-resolution images from low-resolution images, whereas the latter distinguishes between real and generated images. The two networks were trained in an adversarial manner, with the generator network attempting to produce images capable of fooling the discriminator network, and discriminator network attempting to distinguish whether the images were real or not. This adversarial training process helped the generator network learn the mapping between low-resolution and high-resolution images. The 3D SR reconstruction process used in this study is depicted in Fig. 2. Details of SR reconstruction process are provided in Supplementary E3.

In this study, the SR images were obtained from the Onekey platform (version 3.1, Beijing, China) using transfer learning. The 3D SR reconstruction technique utilized in this study has shown promising results, leading to a four-fold increase in the spatial resolution of medical images, while maintaining the original image size. This means that a pixel volume of $1 \times 1 \times 1$ mm^3 can be transformed into a $1 \times 1 \times 0.25$-mm^3 volume. The technique has been evaluated based on various medical imaging modalities, including CT, magnetic resonance imaging, and ultrasonography, significantly improving image quality and spatial resolution. The technique has also been compared with other state-of-the-art SR reconstruction techniques and has shown superior performance [13].

2.5. Image segmentation

Two radiologists (readers 1 and 2, with 5 and 12 years of experience in cardiovascular imaging, respectively) who were blinded to all the clinical information performed the image segmentation. Manual segmentation of all plaque volumes of interest was independently performed by reader 1 on both normal-resolution (NR) and SR slices using open-source ITK-SNAP software (version 3.8.0, www.itksnap.org). Plaques in the narrowest part of the carotid lumen were manually delineated on axial slices. To assess the inter-rater reliability during plaque segmentation process, the target carotid plaques were re-outlined by readers 1 and 2 in 40 randomly selected patients 2 weeks later. Intraclass correlation coefficients were also calculated.

2.6. Radiomic feature extraction and selection

Images were preprocessed to facilitate feature reproducibility and eliminate variance caused by different acquisition parameters. All images were resampled to a standardized voxel size of $1 \times 1 \times 1$ mm^3 using a B-spline interpolation algorithm, the voxel intensity values discretized, with a fixed bin width of 32 units, and the window width and level set to 350 and 70 respectively. Subsequently, the radiomic features of the segmented NR and SR images were extracted based on 3D volumes of interest using the pyradiomics software package (version 3.1.0) on the Python (version 3.7) platform.

Handcrafted features can be categorized into three groups according to geometry, intensity, and texture. Geometry features describe the geometric properties of a plaque, such as its volume, surface area, and eccentricity. Intensity features capture the distribution and intensity values of the plaque on imaging. Finally, texture features quantify the spatial arrangement of voxel intensities within the plaque, providing information about its heterogeneity and composition.

After all the radiomic features were z-standardized to obtain a normal distribution, feature selection was performed according to the following four-step procedure: (1) Intraclass correlation coefficients were calculated to evaluate the inter- and intra-observer reliability, and the radiomic features with coefficients >0.85 were selected. (2) Pearson's correlation coefficients were calculated to assess correlations between highly repetitive features; if the absolute value of the correlation coefficient was >0.9 between any two features, only one was retained. (3) The least absolute shrinkage and selection operator method with 5-fold cross-validation was used to identify the features with nonzero coefficients, depending on the tuning of the regularization parameter (λ) based on the minimum criteria. (4) The voting method was used for the final feature selection. To ensure the reliability of the selected features, steps 2 and 3 were looped five times using a 5-fold cross-validation framework, and the features that appeared more than three times were retained for model development.

2.7. Risk model development and evaluation

The final radiomic features were input into the machine learning models for the identification of symptomatic carotid plaques. A support vector machine (SVM) algorithm with a radial basis kernel was adopted for a risk model development using 5-fold cross-validation. As shown in Fig. 3, the model training and evaluation steps were also based on a 5-fold cross-validation framework to avoid the possible sampling associated with the arbitrary splitting of data and to reduce the prediction error variance. First, the overall datasets were randomly divided into five similarly sized, nonoverlapping groups. One group containing 20% of all data was used as the test set, whereas the remaining 80% was used in the other groups as the training set. The training set was used for radiomic feature selection and model development, and the model performance was evaluated using the test set. This procedure was looped five times over the various groups, meaning different training and test sets were used for feature selection and model development each time, and no data were used for both the training and testing sets simultaneously. After the loop was completed, the five models were stacked to evaluate their overall performance ability in identifying symptomatic carotid atherosclerotic plaques.

Receiver operating characteristic curves were plotted, the area under the receiver operating characteristic curve (AUC) values calculated to evaluate the discrimination performance of the risk models, and receiver operating characteristic curves compared using the DeLong test. The accuracy, sensitivity, specificity, positive predictive value, negative predictive value, precision, and F1 scores of each model were compared and analyzed. Calibration curves and the Hosmer–Lemeshow test were used to evaluate the goodness of fit of the risk models; a non-significant test statistic indicated good calibration. Decision curve analysis was conducted to assess the utility of the models for clinical decision-making.

2.8. Statistical analysis

Data for continuous variables are presented as the mean ± standard deviation. The Shapiro–Wilk test was used to examine whether the assumption of normal distribution was violated; for variables in which it was not, the data were compared between two groups using the Student's *t*-test. In cases where the assumption of normality was violated, the non-parametric Mann–Whitney *U* test was used to compare data between two groups. Data for categorical variables are expressed as frequencies and percentages and were compared using the chi-square test. A two-tailed p-value <0.05 was considered statistically significant. All statistical analyses were performed using SPSS (version 25.0, IBM) and Python (version 3.7).

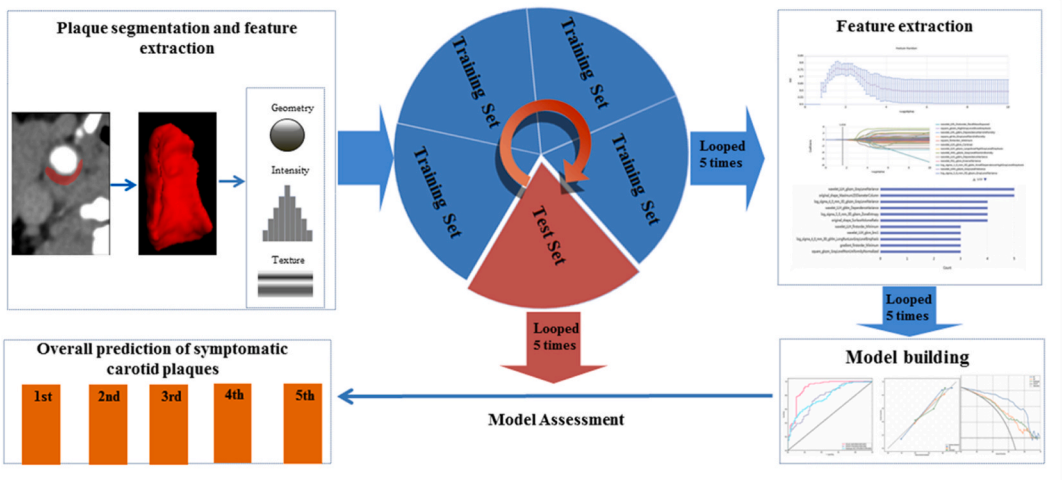

Fig. 3. Workflow of the radiomic methods used in this study.

3. Results

3.1. Clinical and conventional CTA characteristics of patients

According to the inclusion criteria, 556 patients with carotid atherosclerosis diagnosed using head-and-neck CTA were eligible for inclusion; however, 363 patients were removed based on the exclusion criteria (Fig. 1). Ultimately, 193 patients were enrolled, 123 of whom were allocated to the symptomatic group (age: 64.06 ± 8.76 years old; 25 women and 98 men) and 70 of whom were allocated to the asymptomatic group (age: 63.07 ± 11.60 years old; 11 women and 59 men). Data for

all clinical and conventional CTA variables are summarized in Table 1.

3.2. Radiomic feature selection

Fourteen geometry, 18 intensity, and 68 texture features were assessed. After applying 19 image filters for intensity and texture features, 1,648 (i.e., 19 × [68 + 18] + 14) handcrafted features (Supplementary Tables S1 and S2) were extracted according to the imaging biomarker standardization initiative criteria (IBSI). The feature selection process was implemented using the uAI Research Portal (https://urp.united-imaging.com, version 20230715). Finally, 4 conventional quantitative CTA features measured by radiologists, 5 NR features, and 18 SR features were retained after voting using a 5-fold cross-validation framework (Supplementary Fig. S1).

3.3. Risk model performance evaluation

In the training cohort (Fig. 4A), the radiologist model based on quantitative CTA characteristics, NR model, and SR model yielded AUCs of 0.776 (95% CI 0.709–0.842), 0.769 (95% CI 0.699–0.838), and 0.907 (95% CI 0.857–0.957), respectively. In the testing cohort (Fig. 4B), the SR model exhibited an AUC of 0.820 (95% CI 0.756–0.884), indicating that performed better than the NR and radiologist models, which had AUCs of 0.711 (95% CI 0.633–0.789) and 0.677 (95% CI 0.600–0.753), respectively. The DeLong test (Supplementary Fig. S2) revealed a statistically significant difference in the receiver operating characteristic curves between the SR model and both the NR and radiologist models in both the training and testing cohorts. Table 2 shows the three models' evaluation results, including the accuracy, sensitivity, specificity, positive predictive value, negative predictive value, precision, and F1 score.

In both the training and testing cohorts, the calibration curves (Fig. 4C and D) indicated that the SR model exhibited superior agreement compared with that of the other two models in identifying symptomatic carotid plaque. Additionally, the Hosmer–Lemeshow test results (Table 2) revealed no deviations from a perfect fit for all three models in both cohorts (all $p > 0.05$).

Furthermore, as illustrated in Fig. 4E and F, the decision curves analysis demonstrated that the application of the NR model could enhance the clinical benefits for patients compared with the radiologist model, whereas application of the SR model could provide greater benefits to patients than either of the other models.

Table 1
Clinical and imaging characteristics of patients.

	Total (n = 193)	Symptomatic group (n = 123)	Asymptomatic group (n = 70)	P value
Clinical characteristics				
Gender, Male	157 (81.3%)	98 (79.7%)	59 (84.3%)	0.429
Age, y	63.7 ± 9.87	64.06 ± 8.76	63.07 ± 11.60	0.538
BMI, kg/m^2	24.10 ± 3.21	24.13 ± 3.18	24.05 ± 3.27	0.769
Smoking	87 (45.1%)	62 (50.4%)	25 (35.7%)	0.049*
Drinking	33 (17.1%)	21 (17.1%)	12 (17.1%)	0.990
Hypertension	147 (76.2%)	98 (79.7%)	49 (70.0%)	0.129
Diabetes	76 (39.4%)	49 (39.8%)	27 (38.6%)	0.863
Glycosylated hemoglobin, %	6.57 ± 1.52	6.52 ± 1.66	6.66 ± 1.24	0.066
TG, mmol/L	1.62 ± 0.84	1.68 ± 0.94	1.52 ± 0.60	0.151
TC, mmol/L	4.23 ± 1.19	4.31 ± 1.30	4.07 ± 0.95	0.366
HDL-C, mmol/L	1.07 ± 0.25	1.07 ± 0.26	1.07 ± 0.24	0.887
LDL-C, mmol/L	2.64 ± 0.88	2.74 ± 0.96	2.46 ± 0.71	0.103
Conventional CTA characteristics				
Lumen stenosis, %	46.83 ± 15.53	50.25 ± 15.17	40.80 ± 14.39	<0.001*
Plaque ulceration	42 (21.8%)	36 (29.3%)	6 (8.6%)	<0.001*
CT Value, HU	26.65 ± 9.60	26.11 ± 9.73	27.59 ± 9.37	0.253
Max soft-plaque thickness, mm	3.35 ± 0.86	3.51 ± 0.84	3.06 ± 0.84	<0.001*
Max soft-plaque length, mm	22.16 ± 7.92	22.34 ± 8.30	21.85 ± 7.24	0.890
Minimum luminal area, mm^2	14.99 ± 9.19	13.45 ± 9.34	17.69 ± 8.32	<0.001*

NOTE. Continuous variables are presented as mean ± standard deviation and categorical variables are presented as numbers with percentages in parentheses. BMI, body mass index. TG, triglyceride. TC, total cholesterol. HDL-C, high-density lipoprotein cholesterol. LDL-C, low-density lipoprotein cholesterol. *P value < 0.05.

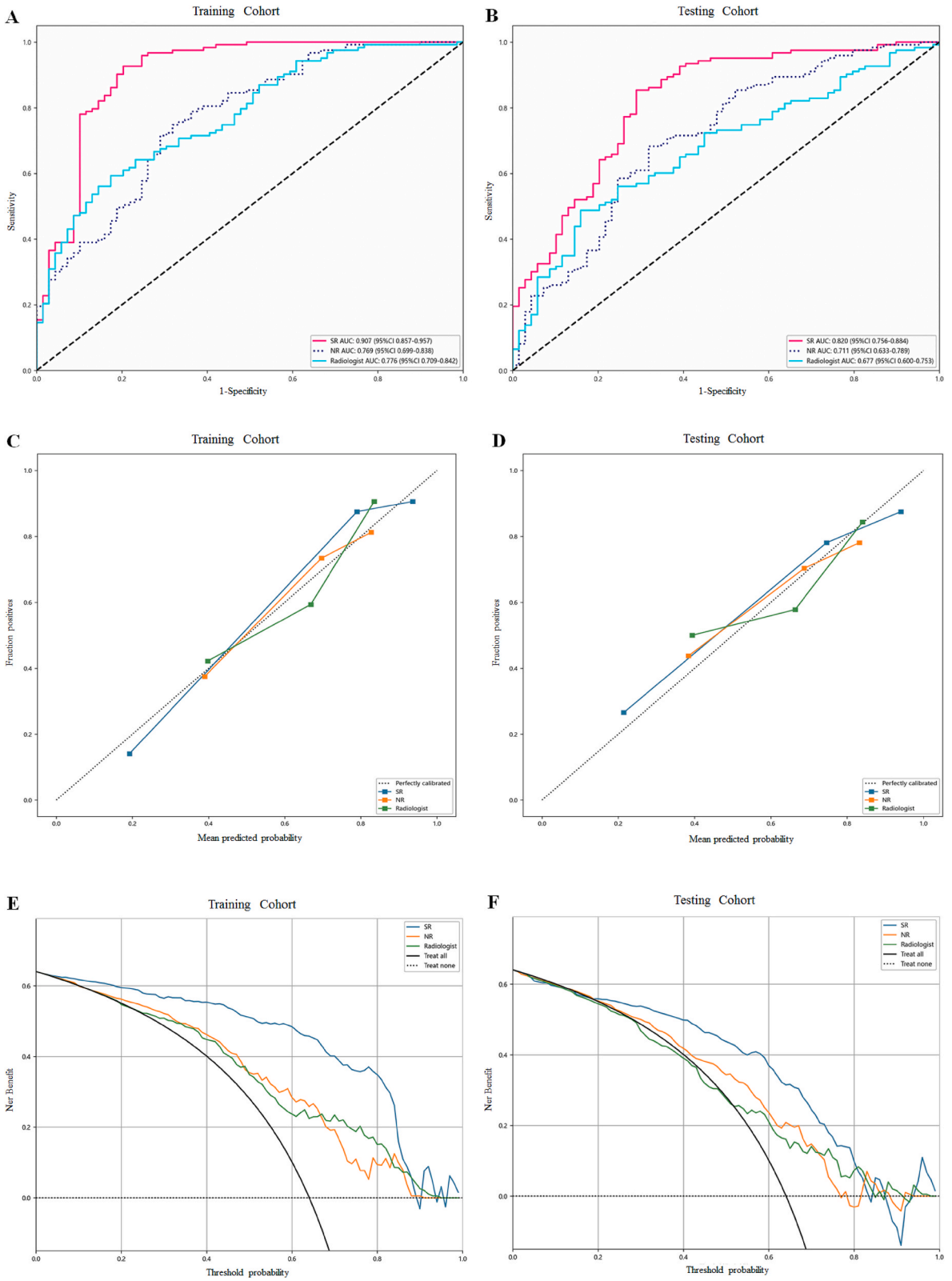

Fig. 4. Performance assessment of the three models. Receiver operating characteristic curves of the models in the training (A) and testing (B) cohorts. The calibration curves of the models using data from the training (C) and testing (D) cohorts. Decision curve analysis for the models in the training (E) and testing (F) cohorts.

Table 2
Performance of risk models for identification of symptomatic carotid.

Models	Cohort	Accuracy	AUC (95% CI)	Sensitivity	Specificity	PPV	NPV	Precision	F1 score	Hosmer-Lemeshow test
SR	Training	0.880	0.907 (0.8571–0.9572)	0.927	0.797	0.891	0.859	0.891	0.908	0.261
SR	Testing	0.802	0.820 (0.7560–0.8844)	0.854	0.71	0.84	0.731	0.84	0.847	0.369
NR	Training	0.724	0.769 (0.6989–0.8383)	0.748	0.681	0.807	0.603	0.807	0.776	0.068
NR	Testing	0.682	0.711 (0.6334–0.7887)	0.683	0.681	0.792	0.547	0.792	0.734	0.525
Radiologist	Training	0.677	0.776 (0.7094–0.8422)	0.593	0.826	0.859	0.533	0.859	0.702	0.159
Radiologist	Testing	0.615	0.677 (0.5998–0.7533)	0.488	0.841	0.845	0.479	0.845	0.619	0.663

NOTE. SR, super-resolution. NR, normal-resolution. PPV, positive predictive value. NPV, negative predictive value. AUC, area under the curve.

4. Discussion

In this study, SR head-and-neck CTA images were generated using a deep learning model based on generative adversarial network architecture, and a radiomic risk model based on SR CTA images was developed and evaluated. The enhanced SR image quality had several advantages. Compared to that of the other two models based on NR CTA images and manually quantified CTA features, the SR radiomic model exhibited significantly better performance for symptomatic carotid plaque identification.

Since the carotid plaque composition plays a crucial role in the atherosclerotic stroke development, the traditional diagnostic strategy based solely on the degree of luminal stenosis is inadequate [4]. Symptomatic carotid plaques are a manifestation of advanced atherosclerosis and are composed of thinner fibrous caps and larger, lipid-rich necrotic cores, with more inflammatory components than asymptomatic carotid plaques [2,12]. These plaques are also more fragile and prone to rupture, potentially triggering downstream thrombus formation and acute cerebrovascular events [2,4,12]. Therefore, identifying symptomatic carotid plaques is critical for ensuring early and accurate assessments of the risk of future stroke events and facilitating clinical decision-making.

High-resolution magnetic resonance vessel wall imaging can help accurately visualize the morphology and composition of carotid plaques, including areas of intra-plaque hemorrhage and the lipid-rich necrotic core [3,31,32], and positron emission tomography-CT can provide information about the inflammation-related metabolism of carotid plaques [33,34]. Although these technologies can help identify symptomatic carotid plaques, the process is complex and time-consuming, and the relatively high number of contraindications of the techniques limit their widespread clinical applications in this context [10]. CTA has been widely utilized for carotid plaque analysis in clinical practice due to its greater convenience compared to that of magnetic resonance imaging and positron emission tomography-CT, and it can assess the degree of carotid artery stenosis and characterize plaque morphology, evaluate plaque composition by distinguishing between calcified and non-calcified components, and clearly identify areas of plaque ulceration [4,10,31].

Radiomics is a rapidly evolving field in medical imaging, and studies have confirmed its applications and potential in guiding clinical decision-making and precision medicine [25]. Radiomics-based carotid artery CTA methodologies are an objective and effective means of assessing carotid atherosclerotic plaques and stratifying related risk [35]. However, the accuracy and reliability of CT-based radiomic analyses are heavily dependent on the quality of acquired images, and routine carotid artery CTA images are usually of low resolution, possibly leading to inaccurate feature extraction and subsequent risk evaluation [24].

SR techniques can significantly enhance the quality of low-resolution images by generating high-resolution versions of them. Various techniques are employed for SR reconstruction, including deep learning-based approaches and some traditional methods that include interpolation-based techniques such as bilinear and bicubic interpolation. Although these traditional approaches are simple and efficient, they typically rely on information from neighboring pixels to estimate missing high-frequency details, sometimes leading to artifacts or image blurring [36]. In contrast, deep learning-based SR reconstruction techniques have gained increasing attention in recent years, because they permit end-to-end training, enabling the direct mapping of low-resolution to SR images without intermediate steps, eliminating tedious manual parameter adjustments and the reliance on engineers' experience, thereby saving time and resources [13]. In the present study, a novel deep learning-based SR reconstruction strategy utilizing generative adversarial networks was implemented to enhance the resolution of head-and-neck CTA images. As shown in Fig. 2, the enlarged SR images exhibited no jagged edges or blurring, permitting the successful visualization of minute details within carotid plaques due to increased image sharpness compared to that of the NR images. Moreover, the accuracy of handcrafted lesion segmentation within a region of interest was greatly improved in the SR images.

Although SR images have better spatial resolution, it remains unclear whether that can be helpful for radiomics-based clinical analyses of carotid plaques. In many previous studies, deep learning-based SR reconstruction methods have been applied to various medical image types [37–41], significantly improving the robustness of radiomic features compared to those based on traditional SR methods [14,24]. In the present study, two radiomic models based on SR and NR CTA images and a model based on quantitative CTA parameters manually measured by radiologists were developed for identifying symptomatic carotid plaques. To minimize the risk of model overfitting resulting from random division of the dataset and assess more accurately and objectively the improvement of the

radiomic by super-resolution reconstruction, a 5-fold cross-validation framework was adopted for model training and testing. The predictions of the corresponding five models were stacked to evaluate the overall prediction performance of the models in this study.

Although there was no statistically significant difference in the AUC values between the NR radiomic model and radiologist model, the former performed better than the latter, with improved accuracy and sensitivity, and a higher F1 score. These findings may be because the quantitative CTA parameters were measured by radiologists based on manually selected regions of interest within the plaque based on 2D images, which may not have accurately reflected the overall composition or environment within the plaque, whereas the radiomic features were automatically extracted from volumes of interest within the plaque, allowing for more stable, accurate, and objective evaluations.

Radiomic texture features, such as the gray level co-occurrence matrix (GLCM), gray level dependence matrix (GLDM), gray level run length matrix (GLRLM), and gray level size zone (GLSZM), provide more information about the heterogeneity of plaques [42]. The effectiveness of radiomic texture features in distinguishing between symptomatic and asymptomatic plaques has been demonstrated [21,23,35]. The higher the image resolution, the clearer the details in the image, and the richer the texture feature information, resulting in more accurate and reliable texture feature extraction and analysis results. In this study, following feature selection, more radiomic features, especially texture features, based on SR images were retained for model development compared to those based on NR images. Additionally, the surface morphology of plaque is also a crucial indicator of high-risk plaques [4]. Carotid plaques with irregular surface morphology are considered to be associated with an increased risk of stroke [43]. This study showed that two shape features, namely “SurfaceVolumeRatio” and “Sphericity,” were ultimately retained based on SR images. The two radiomic features are commonly used to describe the geometric characteristics of ROI in images, reflecting the complexity of its surface and spatial distribution. The utilization of high-resolution images enables the capture of finer details and more comprehensive information regarding surface morphology of plaques, thereby improving the accuracy of calculating the values of these two features. The aforementioned findings confirm that deep learning-based SR reconstruction methods can both enhance image quality to display greater detail of the plaque composition and morphology and vastly improve the performance of radiomic models for carotid plaque risk assessment. Moreover, the SR radiomic model demonstrated even greater performance in identifying symptomatic carotid plaques, with significantly higher AUC and accuracy values than those of the other two models, and the decision curve analysis revealed significantly improved patient benefits with the SR model.

This study has several limitations. First, although this was a single-center study, a 5-fold cross-validation framework was used in the model development process to overcome some of the associated limitations; however, the absence of external validation may have limited the generalizability of the modeling in different populations. Second, the small sample size and retrospective nature of the study may have biased the results; therefore, a prospective multicenter study should be designed and conducted. Third, manual segmentation depends on the radiologists’ individual experiences and perceptions, possibly affecting the values applied to certain radiomic features. Deep learning automatic segmentation will be applied in subsequent studies to reduce subjective interference and improve outcomes based on radiomic features. Despite these limitations, the deep learning-based SR reconstruction method used in this study significantly improved the performance of the radiomic model in identifying symptomatic carotid plaques.

5. Conclusion

The deep learning-based 3D SR radiomic model for identifying symptomatic carotid plaques developed and evaluated in this study outperformed those based on NR radiomic features or conventional quantitative CTA parameters. The utilization of this technique can significantly improve the display details of carotid plaque, thus holding great potential in enhancing the detection accuracy of radiomics models for carotid symptomatic plaques and assisting clinical decision-making.

Ethical approval

This study was approved by the institutional review board of the First Hospital of Shanxi Medical University (no. 2018K008) and the requirement for informed consent was waived because of the retrospective design.

Data availability statement

The data supporting the findings of this study are available from the corresponding author upon reasonable request.

Funding

This work was financially supported by the Fundamental Research Program of Shanxi Province (Nos. 20210302123253 and 20210302123256), Science and Technology Plan Project of Inner Mongolia Autonomous Region (No. 2020GG0106) and Natural Science Foundation of Inner Mongolia Autonomous Region (No. 2023MS08047).

CRediT authorship contribution statement

Lingjie Wang: Writing – original draft, Conceptualization. **Tiedan Guo:** Data curation. **Li Wang:** Data curation. **Wentao Yang:** Data curation. **Jingying Wang:** Formal analysis. **Jianlong Nie:** Visualization, Validation, Methodology. **Jingjing Cui:** Visualization, Validation, Methodology. **Pengbo Jiang:** Visualization, Validation, Methodology. **Junlin Li:** Writing – original draft. **Hua Zhang:**

Writing – review & editing, Supervision.

Declaration of competing interest

The authors declare that they have no known competing financial interests or personal relationships that could have appeared to influence the work reported in this paper.

Acknowledgements

We appreciate the United Imaging Intelligence and OnekeyAI teams for their assistance in this study. We would like to thank Editage (www.editage.cn) for English language editing.

Appendix A. Supplementary data

Supplementary data to this article can be found online at https://doi.org/10.1016/j.heliyon.2024.e29331.

References

[1] D. van Dam-Nolen, N. van Egmond, P.J. Koudstaal, A. van der Lugt, D. Bos, Sex differences in carotid atherosclerosis: a systematic review and meta-analysis, Stroke 54 (2) (2023) 315–326.
[2] J. Golledge, R.M. Greenhalgh, A.H. Davies, The symptomatic carotid plaque, Stroke 31 (3) (2000) 774–781.
[3] D. van Dam-Nolen, M. Truijman, A.G. van der Kolk, et al., Carotid plaque characteristics predict recurrent ischemic stroke and TIA: the PARISK (plaque at RISK) study, JACC Cardiovasc Imaging 15 (10) (2022) 1715–1726.
[4] L. Saba, T. Saam, H.R. Jäger, et al., Imaging biomarkers of vulnerable carotid plaques for stroke risk prediction and their potential clinical implications, Lancet Neurol. 18 (6) (2019) 559–572.
[5] P.M. Rothwell, M. Eliasziw, S.A. Gutnikov, et al., Analysis of pooled data from the randomised controlled trials of endarterectomy for symptomatic carotid stenosis, Lancet 361 (9352) (2003) 107–116.
[6] L. Saba, C. Yuan, T.S. Hatsukami, et al., Carotid artery wall imaging: perspective and guidelines from the ASNR vessel wall imaging study group and expert consensus recommendations of the American Society of Neuroradiology, AJNR Am J Neuroradiol 39 (2) (2018) E9–E31.
[7] V. Aboyans, J.B. Ricco, M. Bartelink, et al., 2017 ESC guidelines on the diagnosis and treatment of peripheral arterial diseases, Eur. Heart J. 39 (9) (2018) 763–816, in collaboration with the European Society for Vascular Surgery (ESVS): Document covering atherosclerotic disease of extracranial carotid and vertebral, mesenteric, renal, upper and lower extremity arteriesEndorsed by: the European Stroke Organization (ESO)The Task Force for the Diagnosis and Treatment of Peripheral Arterial Diseases of the European Society of Cardiology (ESC) and of the European Society for Vascular Surgery (ESVS).
[8] P.J. Homburg, S. Rozie, M.J. van Gils, et al., Atherosclerotic plaque ulceration in the symptomatic internal carotid artery is associated with nonlacunar ischemic stroke, Stroke 41 (6) (2010) 1151–1156.
[9] H. Baradaran, K. Al-Dasuqi, A. Knight-Greenfield, et al., Association between carotid plaque features on CTA and cerebrovascular ischemia: a systematic review and meta-analysis, AJNR Am J Neuroradiol 38 (12) (2017) 2321–2326.
[10] H. Baradaran, L.B. Eisenmenger, P.J. Hinckley, et al., Optimal carotid plaque features on computed tomography angiography associated with ischemic stroke, J. Am. Heart Assoc. 10 (5) (2021) e019462.
[11] Q. Yang, H. Guo, X. Shi, et al., Identification of symptomatic carotid artery plaque: a three-item scale combined angiography with optical coherence tomography, Front. Neurosci. 15 (2021) 792437.
[12] D.P. Howard, G.W. van Lammeren, P.M. Rothwell, et al., Symptomatic carotid atherosclerotic disease: correlations between plaque composition and ipsilateral stroke risk, Stroke 46 (1) (2015) 182–189.
[13] M. Fan, Z. Liu, M. Xu, et al., Generative adversarial network-based super-resolution of diffusion-weighted imaging: application to tumour radiomics in breast cancer, NMR Biomed. 33 (8) (2020) e4345.
[14] M. Hou, L. Zhou, J. Sun, Deep-learning-based 3D super-resolution MRI radiomics model: superior predictive performance in preoperative T-staging of rectal cancer, Eur. Radiol. 33 (1) (2023) 1–10.
[15] M.L. de Leeuw den Bouter, G. Ippolito, T. O'Reilly, R.F. Remis, M.B. van Gijzen, A.G. Webb, Deep learning-based single image super-resolution for low-field MR brain images, Sci. Rep. 12 (1) (2022) 6362.
[16] J. Liao, J. Qu, Y. Hao, J. Li, Deep-learning-based methods for super-resolution fluorescence microscopy, J. Innov. Opt. Health Sci. 16 (3) (2023).
[17] H. Almansour, S. Gassenmaier, D. Nickel, et al., Deep learning-based superresolution reconstruction for upper abdominal magnetic resonance imaging: an analysis of image quality, diagnostic confidence, and lesion conspicuity, Invest. Radiol. 56 (8) (2021) 509–516.
[18] J.E. van Timmeren, D. Cester, S. Tanadini-Lang, H. Alkadhi, B. Baessler, Radiomics in medical imaging-"how-to" guide and critical reflection, Insights Imaging 11 (1) (2020) 91.
[19] Y.Q. Huang, C.H. Liang, L. He, et al., Development and validation of a radiomics nomogram for preoperative prediction of lymph node metastasis in colorectal cancer, J. Clin. Oncol. 34 (18) (2016) 2157–2164.
[20] D. Dong, M.J. Fang, L. Tang, et al., Deep learning radiomic nomogram can predict the number of lymph node metastasis in locally advanced gastric cancer: an international multicenter study, Ann. Oncol. 31 (7) (2020) 912–920.
[21] F. Zaccagna, B. Ganeshan, M. Arca, et al., CT texture-based radiomics analysis of carotid arteries identifies vulnerable patients: a preliminary outcome study, Neuroradiology 63 (7) (2021) 1043–1052.
[22] Z. Dong, C. Zhou, H. Li, et al., Radiomics versus conventional assessment to identify symptomatic participants at carotid computed tomography angiography, Cerebrovasc. Dis. 51 (5) (2022) 647–654.
[23] R. Zhang, Q. Zhang, A. Ji, et al., Identification of high-risk carotid plaque with MRI-based radiomics and machine learning, Eur. Radiol. 31 (5) (2021) 3116–3126.
[24] E.C. de Farias, C. di Noia, C. Han, E. Sala, M. Castelli, L. Rundo, Impact of GAN-based lesion-focused medical image super-resolution on the robustness of radiomic features, Sci. Rep. 11 (1) (2021) 21361.
[25] J. Zhong, Y. Xia, Y. Chen, et al., Deep learning image reconstruction algorithm reduces image noise while alters radiomics features in dual-energy CT in comparison with conventional iterative reconstruction algorithms: a phantom study, Eur. Radiol. 33 (2) (2023) 812–824.
[26] L. Saba, S. Zucca, A. Gupta, et al., Perivascular fat density and contrast plaque enhancement: does a correlation exist, AJNR Am J Neuroradiol 41 (8) (2020) 1460–1465.

[27] R.L. Sacco, S.E. Kasner, J.P. Broderick, et al., An updated definition of stroke for the 21st century: a statement for healthcare professionals from the American Heart Association/American Stroke Association, Stroke 44 (7) (2013) 2064–2089.
[28] North American symptomatic carotid endarterectomy trial. Methods, patient characteristics, and progress, Stroke 22 (6) (1991) 711–720.
[29] V. Rafailidis, I. Chryssogonidis, T. Tegos, K. Kouskouras, A. Charitanti-Kouridou, Imaging of the ulcerated carotid atherosclerotic plaque: a review of the literature, Insights Imaging 8 (2) (2017) 213–225.
[30] C. Ledig, L. Theis, F. Huszár, et al., Photo-realistic single image super-resolution using a generative adversarial network. Proceedings of the IEEE Conference on Computer Vision and Pattern Recognition, 2017, pp. 4681–4690.
[31] A. Huibers, G.J. de Borst, S. Wan, et al., Non-invasive carotid artery imaging to identify the vulnerable plaque: current status and future goals, Eur. J. Vasc. Endovasc. Surg. 50 (5) (2015) 563–572.
[32] B. Sun, X. Li, X. Liu, et al., Association between carotid plaque characteristics and acute cerebral infarction determined by MRI in patients with type 2 diabetes mellitus, Cardiovasc. Diabetol. 16 (1) (2017) 111.
[33] P.J. Kelly, P. Camps-Renom, N. Giannotti, et al., Carotid plaque inflammation imaged by 18F-fluorodeoxyglucose positron emission tomography and risk of early recurrent stroke, Stroke 50 (7) (2019) 1766–1773.
[34] P.J. Kelly, P. Camps-Renom, N. Giannotti, et al., A risk score including carotid plaque inflammation and stenosis severity improves identification of recurrent stroke, Stroke 51 (3) (2020) 838–845.
[35] S. Cilla, G. Macchia, J. Lenkowicz, et al., CT angiography-based radiomics as a tool for carotid plaque characterization: a pilot study, Radiol. Med. 127 (7) (2022) 743–753.
[36] Y. Yan, C. Liu, C. Chen, et al., Fine-grained attention and feature-sharing generative adversarial networks for single image super-resolution, IEEE Trans. Multimed. 24 (2021) 1473–1487.
[37] O. Oktay, W. Bai, M. Lee, et al., Multi-input cardiac image super-resolution using convolutional neural networks, Medical Image Computing and Computer-Assisted Intervention-MICCAI 2016: 19th International Conference, Athens, Greece, October 17-21, 2016, Proceedings, Part III 19 (2016) 246–254.
[38] C. Pham, C. Tor-Díez, H. Meunier, et al., Multiscale brain MRI super-resolution using deep 3D convolutional networks, Comput. Med. Imag. Graph. 77 (2019) 101647.
[39] K. Zeng, H. Zheng, C. Cai, Y. Yang, K. Zhang, Z. Chen, Simultaneous single-and multi-contrast super-resolution for brain MRI images based on a convolutional neural network, Comput. Biol. Med. 99 (2018) 133–141.
[40] Y. Li, F. Xu, F. Zhang, et al., DLBI: deep learning guided Bayesian inference for structure reconstruction of super-resolution fluorescence microscopy, Bioinformatics 34 (13) (2018) i284–i294.
[41] A. Juhong, B. Li, C.Y. Yao, et al., Super-resolution and segmentation deep learning for breast cancer histopathology image analysis, Biomed. Opt Express 14 (1) (2023) 18–36.
[42] M. Liu, N. Chang, S. Zhang, et al., Identification of vulnerable carotid plaque with CT-based radiomics nomogram, Clin. Radiol. 78 (11) (2023) e856–e863.
[43] H.J. Barnett, D.W. Taylor, M. Eliasziw, et al., Benefit of carotid endarterectomy in patients with symptomatic moderate or severe stenosis. North American Symptomatic Carotid Endarterectomy Trial Collaborators, N. Engl. J. Med. 339 (20) (1998) 1415–1425.